Frequency Correlation of QPOs Based on a Resonantly-Excited Disk-Oscillation Model

Shoji Kato
2-2-2 Shikanodai-Nishi, Ikoma-shi, Nara, 630-0114
kato.shoji@gmail.com, kato@kusastro.kyoto-u.ac.jp

(Received 2008 0; accepted 2008 0)

Abstract

In previous papers, we have proposed a model that the high-frequency quasi-periodic oscillations (HF QPOs) observed in black-hole and neutron-star X-ray binaries are inertial-acoustic oscillations that are resonantly excited on a one-armed deformed disk by nonlinear couplings between the oscillations and the disk deformation. In this paper we show that in addition to the inertial-acoustic waves, one-armed corrugation waves are also excited in the deformed disks. They are low-frequency oscillations. We examine frequencies and their correlations among the inertial-acoustic oscillations and the corrugation waves that are excited, in order to know whether they can describe observed frequency correlations among kHz QPOs and low-frequency QPOs (LF QPOs) in neutron-star X-ray binaries. The results seem to well describe the observed correlations in Cir X-1, if we adopt $M = 1.5 \sim 2.0 M_\odot$ and $a_* \sim 0.8$, where M is the mass of the central star and a_* is the dimensionless spin parameter of the metric. Finally, assumptions involved in this disk-oscillation model are briefly summarized and discussed.

Key words: accretion, accretion disks — quasi-periodic oscillations — resonance — spin of central sources — waves — X-rays; stars

1. Introduction

In previous papers (Kato 2004, 2008), we showed that in a *deformed* relativistic Keplerian disk, inertial-acoustic oscillations (and g-mode oscillations) are resonantly excited. The deformation required for the excitation is a warp or a one-armed plane-symmetric spiral pattern.

The inertial-acoustic oscillations resonantly excited in the above deformed disks well describe the 3:2 twin high-frequency quasi-periodic oscillations (HF QPOs) observed in black hole X-ray binaries, if the disk region where the oscillations are excited is surrounded by a hot corona (torus) (Kato and Fukue 2006). In kHz QPOs in neutron-star X-ray binaries,

the frequencies of the twin QPOs change with time with correlation. These correlated time change of twin kHz QPOs can be accounted for, if the deformation has a time-dependent precession (e.g., Kato 2007)[1]. Any successful models of QPOs of neutron-star X-ray binaries, however, should account for the observed frequency correlations not only between twin kHz QPOs but also those among kHz QPOs and low-frequency QPOs (LF QPOs) (Psaltis et al. 1999; Boutloukos et al. 2006).

Concerning disk oscillation modes that are excited in one-armed deformed disks, we find by a careful inspection of mathematical stability analyses by Kato (2008) that the one-armed c-mode oscillations are also resonantly excited in addition of inertial-acoustic oscillations (and g-mode oscillations) (see subsection 4.2). This is of interest in relation to observations, since the one-armed c-mode oscillations have low frequencies and thus they are one of possible candidates of low-frequency QPOs (LF QPOs). Disk oscillations that are excited in one-armed deformed disk are thus inertial-acoustic oscillations (and g-mode oscillation) and c-mode oscillations.

In this paper, we examine frequency-frequency correlations among the disk oscillations that are resonantly excited, in order to compare them with observed correlations of QPOs. The oscillation modes considered here are three oscillation modes, i.e., two basic inertial-acoustic oscillations among excited inertial-acoustic ones and the one-armed c-mode oscillation. Comparisons with observations are made to Cir X-1, since frequencies of twin kHz QPOs and LF QPOs to this source are carefully examined recently (Boutloukos et al. 2006).

2. Overview of Resonantly-Excited Disk-Oscillation Model

We present here the essential part of the model (Kato 2004, 2008), although the model has various variations. The disk we consider is a geometrically thin, relativistic disk.

2.1. Disk Deformation

The disks are assumed to be deformed from an axially-symmetric steady state by some external or internal cause. The deformation is taken to be eccentric in the disk plane, i.e., $m_{\rm d}=1$, where $m_{\rm d}$ is the azimuthal wavenumber of the deformation. Concerning the symmetry of the deformation with respect to the equatorial plane, two cases are considered. One is the case where the deformation has no vertical asymmetry, i.e., $n_{\rm d}=0$, where $n_{\rm d}$ is zero or a positive integer specifying the number of node(s) in the vertical direction. The other is the case where the deformation is asymmetric with respect to the equator, i.e., $n_{\rm d}=1$. The latter deformation (i.e., $m_{\rm d}=1$ and $n_{\rm d}=1$) is a kind of tilt or warp.

The deformation is assumed to have a time-dependent precession, i.e., it rotates in the azimuthal direction with time-dependent angular velocity. The angular velocity of the precession is denoted by $\omega_{\rm p}$. If $\omega_{\rm p}$ is positive the precession is prograde, while it is retrograde

[1] In the paper by Kato (2007), mode identification of disk oscillations to observed QPOs was not relevant. This will be corrected in this paper.

when $\omega_{\rm p} < 0$. In the case of neutron star, unlike the case of black hole, it has a surface, and the disk surrounding the star has strong radiative and magnetic couplings with the star. We assume that this is one of possible causes of time-dependent precession of disks. For example, Pringle (1992, 1996) and Maloney et al. (1996) have shown that radiative force from the central star can lead to corrugation of the disk. Even initially planar disks are unstable to warping (Pringle 1996). Movies made by Pringle and his collaborators show that the disk precession is time-dependent and it can drastically change even the direction of the precession.

2.2. Disk Oscillations

We consider oscillations on the disks described above. Disk oscillations are generally described by (ω, m, n), where ω and m are the angular velocity and azimuthal wavenumber ($m = 0, 1, 2, ...$) of the oscillations, respectively, and n is an integer ($n = 0, 1, 2, ...$) describing the number of node(s) of the oscillations in the vertical direction (see Kato et al 2008 for detailed classification of disk oscillations). For a set of (ω, m, n), there are two different kinds of modes of oscillations, except for the case of $n = 0$. In the case of $n = 0$, we have inertial-acoustic oscillations (p-mode) alone, which consist of nearly horizontal motions (motions in the disk plane). In the case of $n \geq 1$, we have two different modes of oscillations. One is gravity oscillations (g-mode). The other is corrugation waves (c-mode) ($n = 1$) or vertical-acoustic oscillations (vertical p-mode)($n \geq 2$).

The oscillation modes that are treated in this paper are the inertial-acoustic mode ($n = 0$) [and the g-mode[2] ($n \geq 1$)] and the c-mode oscillations ($n = 1$) with $m = 1$.

2.3. Nonlinear Resonant Processes

A nonlinear coupling between the disk deformation characterized by ($\omega_{\rm p}$, $m_{\rm d}$, $n_{\rm d}$) and an oscillation with (ω, m, n) brings about oscillations described by ($\omega \pm \omega_{\rm p}$, $m \pm m_{\rm d}$, $n \pm n_{\rm d}$), where various combinations of $\pm$ are possible. These oscillations are hereafter called intermediate oscillations. These intermediate oscillations have resonant interaction with the disk at particular radii where the dispersion relation of the intermediate oscillations is satisfied. There are two kinds of resonance for the same set of ($\omega \pm \omega_{\rm p}$, $m \pm m_{\rm d}$, $n \pm n_{\rm d}$). In one of them, resonance occurs through horizontal motions, while it occurs through vertical motions in the other one. We call the former resonance a horizontal resonance, while the latter resonance a vertical resonance (Kato 2004, 2008).

After making the resonant interaction with the disk, the intermediate oscillations nonlinearly couple with the deformed part of the disks to feedback to the original oscillation of (ω, m, n) (see figure 1 of Kato 2004). This nonlinear feedback processes amplify or dampen the original oscillations, depending on the types of oscillations and of resonance. Careful stability

[2] In this paper we implicitly consider the g-mode oscillations together with the inertial-acoustic oscillations, since they are treated in the same mathematical framework as the inertial-acoustic waves, except when we consider their propagation region.

analyses have been done by Kato (2008) (see also Kato 2004) in the case where the deformation has no precession, i.e., $\omega_{\rm p} = 0$.

3. Conditions of Resonance and Excitation

Here, we outline how the results derived by Kato (2008) to the case of $\omega_{\rm p} = 0$ are generalized to the case of $\omega_{\rm p} \neq 0$.

3.1. The radius of resonance

As mentioned in the previous section, there are two kinds of resonance, i.e., horizontal and vertical resonances. Hereafter, we restrict our attention only to the horizontal resonance, since in the case of no precession, the resonance that can excite disk oscillations is the horizontal resonance alone (Kato 2004, 2008). In the case of $\omega_{\rm p} = 0$, the condition of the horizontal resonance is $[\omega - (m \pm 1)\Omega]^2 - \kappa^2 = 0$ (Kato 2004, 2008), where Ω is the angular velocity of disk rotation and taken to be the relativistic Keplerian one, $\Omega_{\rm K}$, when its numerical figure is required, since we consider geometrically thin disks. The symbol κ is the epicyclic frequency. If the deformation has a precession, the condition for horizontal resonance is generalized to

$$[(\omega \pm \omega_{\rm p}) - (m \pm 1)\Omega]^2 - \kappa^2 = 0, \tag{1}$$

where arbitrary combination of $\pm$ is allowed. Equation (1) gives resonant radii as functions of ω for a given set of $\omega_{\rm p}$ and m (see figures 1 and 2).

To find whether the resonance excites or dampens the oscillations, we must examine (i) the sign of work done on the oscillations at the resonant radii and (ii) the sign of the wave energy of the oscillations (Kato 2008, see also Kato 2004). For example, if a positive work is done at a resonant radius on an oscillation of a positive energy, the oscillation is amplified.

3.2. Work done on oscillations

Analyses made by Kato (2004, 2008) show that the sign of the work done by resonance on oscillations at a resonant radius is governed by the sign of $\omega - (m \pm 1)\Omega$ at the resonant radius, when the deformation has no precession. Let us denote resonant radii given by equation (1) by $r_{\rm resonance}$ and the work done on oscillations by the resonance at $r_{\rm resonance}$ by W. Then, in the case where the deformation has a precession with angular frequency $\omega_{\rm p}$, we have

$$\mathrm{sign}(W) = -\mathrm{sign}[(\omega \pm \omega_{\rm p}) - (m \pm 1)\Omega]_{\rm resonance}, \tag{2}$$

where $\mathrm{sign}(A)$ represents the sign of A, and the subscript resonance denotes the value at $r_{\rm resonance}$.

The wave energy, E, of oscillations depends on whether the main part of oscillations exist inside or outside the corotation radius defined by $\omega - m\Omega = 0$. If it exists inside the corotation radius, the wave energy is negative. In the case where $E > 0$, the oscillations are excited by resonance, if the work done on the oscillations by resonance is positive ($W > 0$). In

the case of $E < 0$, on the other hand, $W < 0$ excites the oscillations.

3.3. Propagation Region of Oscillations

For oscillations to be excited efficiently, the resonant radius must be in the propagation region of the oscillations. In the case of inertial-acoustic oscillations with ω and m, the propagation region is described by

$$(\omega - m\Omega)^2 - \kappa^2 > 0, \tag{3}$$

while it is

$$(\omega - m\Omega)^2 - \kappa^2 < 0 \tag{4}$$

in the case of g-mode oscillations.

In addition to the inertial-acoustic oscillations and g-mode oscillations, we consider in this paper the c-mode oscillations ($n = 1$) with $m = 1$. Their propagation region is described by (e.g., Kato 2001, Kato et al. 1998, 2008)

$$(\omega - \Omega)^2 - \Omega_\perp^2 < 0, \tag{5}$$

when local approximations are adopted, where $\Omega_\perp$ is the vertical epicyclic frequency (Kato 1990) and slightly smaller than $\Omega (= \Omega_{\rm K})$.

4. Description of Resonantly-Excited Oscillations on Propagation Diagram

Descriptions in the previous section give us necessary materials for specifying the oscillation modes that are really excited by resonance. We now examine this issue by using the so-called propagation diagram of oscillations. If an arbitrarily large precession is allowed, various oscillations can be excited. In order to simplify situations by excluding less realistic cases, we restrict our attention here only to the oscillations that can be excited even in the limit of no precession, and study how the frequencies of such resonantly-excited oscillations are affected by the presence of precession of deformation. That is, we restrict our attention only to horizontal resonance. Cases of inertial-acoustic oscillations (and g-mode oscillations[3]) and c-mode oscillations are considered separately below, since the resonant radii are different in these cases.

4.1. Inertial-acoustic oscillations

Examination of excitation conditions of inertial-acoustic oscillations on the propagation diagram has been made in a previous paper (Kato 2008) in the case of no precession (see figures

[3] The resonant excitation of the g-mode oscillations can be treated together with that of the inertial-acoustic oscillations, as mentioned before, except for the difference of propagation region. Excitation of g-mode oscillations is, however, less interesting compared with that of the inertial-acoustic oscillations, since in their propagation region the co-rotation resonance appears except for special cases, and it dampens the g-mode oscillations (Kato 2003; Li et al. 2003). Hence, hereafter, we do not discuss the g-mode oscillations.

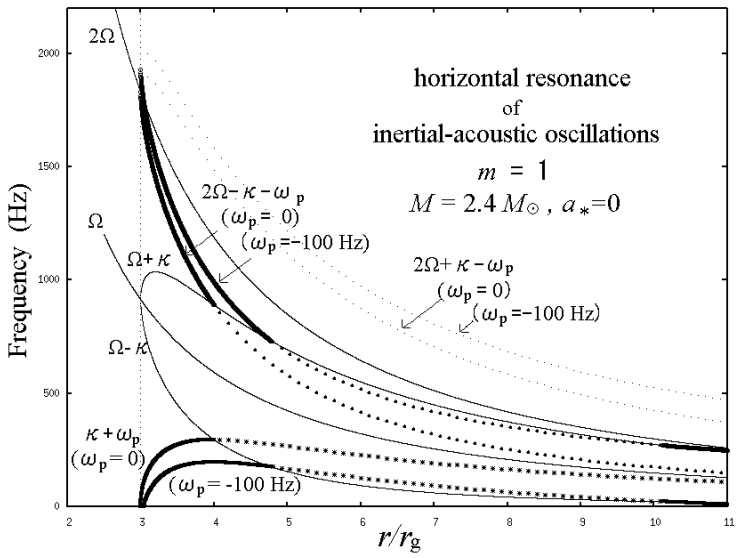

Fig. 1. Propagation diagram (radius-frequency relation) showing the radii and the frequencies of inertial-acoustic oscillations (with $m = 1$) that resonantly interact with a deformed relativistic Keplerian disk. The disk deformation required is a warp or a one-armed plane-symmetric deformation. The mass of the central source is taken to be $2.4M_\odot$ with no spin. Two case are shown where the deformation has no precession ($\omega_{\rm p} = 0$) and has a precession of $\omega_{\rm p} = -100$ Hz. The inside area bounded by two curves labeled by $\Omega + \kappa$ and $\Omega - \kappa$ are the evanescent region of the oscillations. The thick curves (there are two curves for each $\omega_{\rm p}$, and in the case of $\omega_{\rm p} < 0$ they further appear in the right-lower corner of the figure) show the radius-frequency relation of the oscillations that are excited. The thick curves continue in the evanescent regions of oscillations. In the evanescent region, however, excitation of the oscillations will not occur efficiently, and hence the curves in the region are shown by thick but dotted curves. At the boundaries between the propagation and evanescent regions the excitation will occur most efficiently, since the oscillations stay there for a long time because of vanishing of the group velocity. The thin dotted curves show the radius-frequency relation of resonance where oscillations are damped. In the case of gravity oscillations, the propagation region and the evanescent region are opposite to those of the inertial-acoustic oscillations. That is, the evanescent region of the inertial-acoustic oscillations becomes now the propagation region. In other words, in the case of gravity oscillations, the thick dotted curves in figure 1 should be changed to thick curves, and the thick curves to thick dotted ones.

1 and 2 of Kato 2008). Here we extend it to cases where the deformation has precession.

Figure 1 is the frequency-radius relation in the case where oscillations are one-armed (i.e., $m = 1$). The central source is taken to have no spin ($a_* = 0$) and the mass M is $2.4M_\odot$, where a_* is the dimensionless spin parameter specifying the rotation of the metric and $a_* = 1$ corresponds to the extreme Kerr. The inner region bounded by two curves labeled by $\omega = \Omega + \kappa$ and $\omega = \Omega - \kappa$ is the evanescent region of the one-armed inertial-acoustic oscillations [cf., inequality (3)], and the outside of the region is the propagation region of the oscillations. Thick (both solid and dotted) curves give the frequency-radius relation for resonant excitation of one-armed ($m = 1$) inertial-acoustic oscillations [see equation (1) and examine the signs of W and E]. The dotted parts of the thick curves are, however, inside the evanescent region of the

oscillations [see equation (3)], and thus excitation on the part will be practically inefficient. That is, the frequency-radius relations for excitation are the thick solid curves. Two cases of $\omega_{\rm p}=0$ and $\omega_{\rm p}=-100$ Hz are shown. The thin dotted curves are the frequency-radius relation of resonance that leads the oscillations to damping.

As shown in figure 1, one-armed oscillations that are excited are not unique. In a finite range of radius, oscillations are excited with different frequencies [see the sentence just below equation (1)]. Furthermore, two oscillations can be excited at the same radius. One has higher frequencies than Ω at the resonant radius, while the other is smaller than Ω.

Here, we assume that the oscillations whose group velocity is slower will be excited till a larger amplitude than those with a faster group velocity, since they stay a place for a longer time and the resonance condition is maintained for a longer time. If we adopt local approximations, the group velocity of oscillations vanishes at the boundary between the propagation region and the evanescent region, which is specified by $\omega=\Omega+\kappa$ or $\omega=\Omega-\kappa$ in the case of one-armed oscillations. If this consideration is adopted, the most predominantly excited oscillations are those with $\omega=\Omega+\kappa$ in the case of the higher frequency oscillations and those with $\omega=\Omega-\kappa$ in the case of the lower frequency oscillations. Then, combining this condition and the resonant condition given by equation (1), we have, as the condition determining the resonant radius,

$$\kappa=\frac{1}{2}(\Omega-\omega_{\rm p}). \tag{6}$$

If the deformation has no precession, $\omega_{\rm p}=0$, this condition gives $\kappa=\Omega/2$ and the resonance occurs at $4r_{\rm g}$ when the central source has no spin, where $r_{\rm g}$ is the Schwarzschild radius given by $r_{\rm g}=2GM/c^2$. Among a series of resonant radii given by equation (1), the resonant radius given by equation (6) is particularly denoted hereafter by $r_{\rm res}$, which is a function of a_*, M, and $\omega_{\rm p}$.

If we use the notations used so far in the series of our papers, the lower-frequency oscillation at $r_{\rm res}$ is $\omega_{\rm LL}$ and the higher-frequency one is $\omega_{\rm H}$, i.e.,

$$\omega_{\rm LL}=(\Omega-\kappa)_{\rm res} \quad \text{and} \quad \omega_{\rm H}=(\Omega+\kappa)_{\rm res}. \tag{7}$$

Next, we proceed to the two-armed oscillations ($m=2$). Figure 2 is the same as figure 1 except for $m=2$. Two cases of $\omega_{\rm p}=0$ and $\omega=-100$ Hz are again shown for $M=2.4M_\odot$ and $a_*=0$. The thick solid curves and the thick dotted curves are the frequency-radius relations for resonant excitation of oscillations. The thick dotted parts are, however, inside the evanescent region of the oscillations and thus the oscillations in that part will be practically not excited. Thin dotted curves represent the resonance that dampens the oscillations. As in the case of oscillations of $m=1$, the most prominently excited oscillations will be those in which resonance occurs at the boundary between the propagation region and the evanescent region. This consideration again leads to equation (6). Following again the notation used in the previous papers, we denote the frequency of the lower-frequency oscillations at $r_{\rm res}$ and that of the higher-frequency oscillations by $\omega_{\rm L}$ and $\omega_{\rm HH}$, respectively, i.e.,

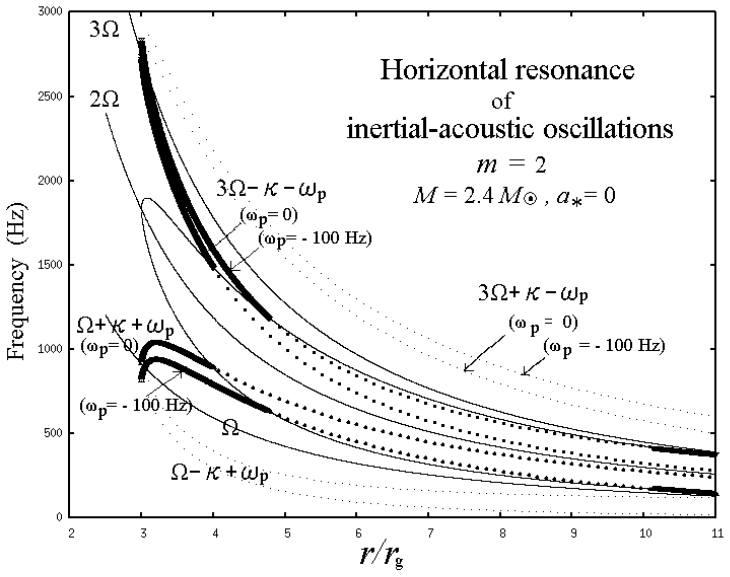

Fig. 2. Same as figure 1 except for $m = 2$. In the present case of $m = 2$, the evanescent region of the oscillations is the inside region bounded by two curves of $2\Omega + \kappa$ and $2\Omega - \kappa$ (these curves are not labeled in the figure in order to avoid complexity).

$$\omega_{\rm L} = (2\Omega - \kappa)_{\rm res} \quad \text{and} \quad \omega_{\rm HH} = (2\Omega + \kappa)_{\rm res}. \tag{8}$$

As figures 1 and 2 show, the curves of the radius-frequency relations for excitation of oscillations (i.e., thick solid or thick dotted curves) cross again, in an outer radius, the boundary curve between the propagation region and the evanescent region when $\omega_{\rm p} = -100$ Hz. In order to show this, the resonant radius, $r_{\rm res}$, obtained by solving equation (6) is shown in figure 3 as a function of $\omega_{\rm p}$ for $a_* = 0.1$ and $a_* = 0.3$ in the case of $M = 2.0 M_\odot$. In figure 3 the $r_{\rm res}$–$\omega_{\rm p}$ relation for the corrugation waves of $m = 1$ is also shown (see the next subsection). [In the case of corrugation waves, the resonant radius is different from $r_{\rm res}$. That is, it is not given by equation (6), but by equation (9) (see the next subsection).]

4.2. C-mode Oscillations

Here, we consider excitation of one-armed corrugation waves (c-mode oscillations) resulting from horizontal resonance. The c-mode oscillations that we consider here are those of $m = 1$. They are a kind of tilt (warp) and have very low frequencies. Their propagation region is specified by equation (5). The boundary of the propagation region, $\omega = \Omega - \Omega_\perp$, in the frequency-radius diagram is shown in figure 4 by a thin solid curve for two cases of $a_* = 0.3$ and $a_* = 0.8$ with $M = 2.0 M_\odot$. In figure 4, the left-hand side of the curve of $\omega = \Omega - \Omega_\perp$ is the propagation region of the one-armed corrugation waves. The right-hand side of the curve is the evanescent region .

The horizontal resonance occurs at the radii where $[(\omega \pm \omega_{\rm p}) - (m \pm 1)\Omega]^2 - \kappa^2 = 0$ is satisfied as mentioned before [see equation (1)]. Examination of the sign of work done on the

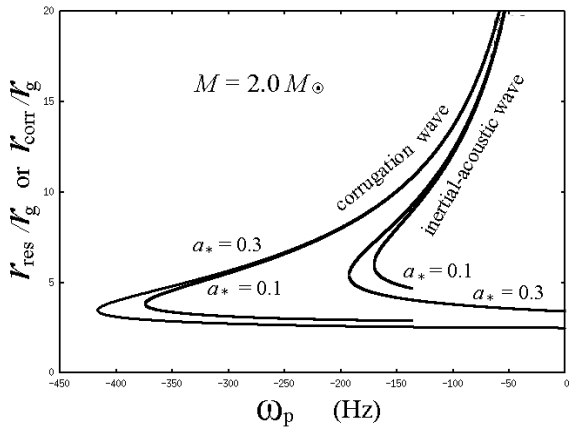

Fig. 3. The relation between resonant radius ($r_{\rm res}$ or $r_{\rm corr}$) and $\omega_{\rm p}$. The relation is shown for inertial-acoustic oscillations and the c-mode oscillations with $m = 1$. Two cases of spin parameter of the central source, i.e., $a_* = 0.1$ and $a_* = 0.3$, are shown with $M = 2.0 M\odot$. It is noted that there are two resonant radii for a given $\omega_{\rm p}$ in the case of $\omega_{\rm p} < 0$. For the case of $a_* = 0$, see figure 1 by Kato and Fukue (2007). In the case of $a_* = 0$, the curve corresponding to the corrugation waves with $m = 1$ disappears in the approximation used in this paper.

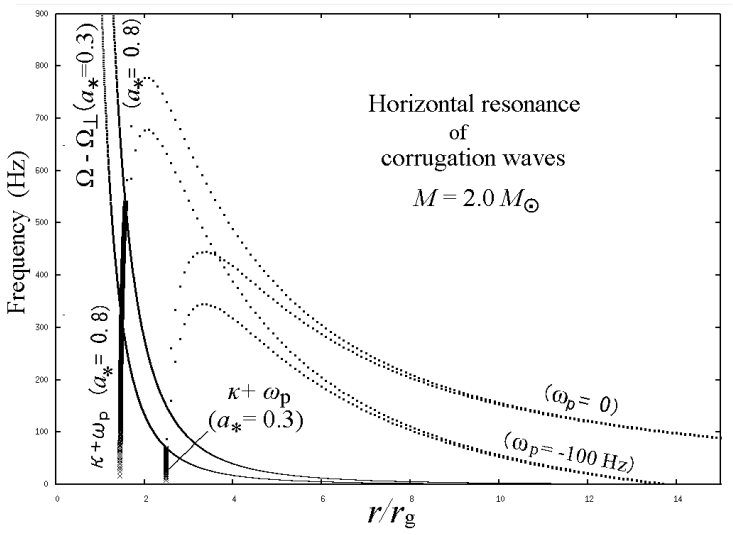

Fig. 4. Propagation diagram showing the radius – frequency relation for resonantly excited corrugation waves with $m = 1$. Two cases of $a_* = 0.3$ and $a_* = 0.8$ are shown for two cases of precession, $\omega_{\rm p} = 0$ and -100 Hz, with $M = 2.0 M\odot$. The curves labelled by $\Omega - \Omega_\perp$ are the boundary between the propagation region and the evanescent region. The left-hand side of the curves are the propagation region. As in figures 1 and 2, the thick solid curves represent the radius – frequency relation where oscillations are excited. Although not shown in this figure, the thick solid curves appear again in the outer region of disks when $\omega_{\rm p} = -100$ Hz (see figure 5).

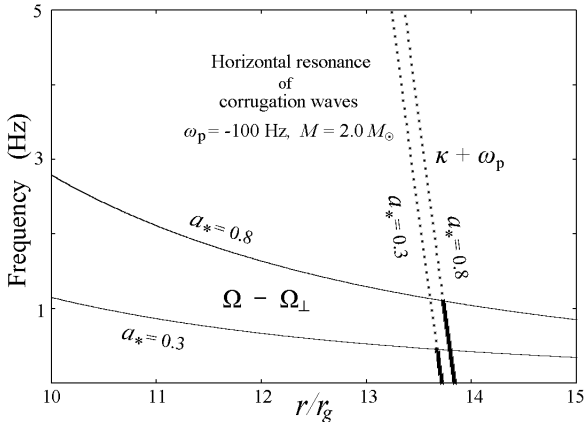

Fig. 5. Enlargement of the lower-right corner of figure 4. Notice that in the case of $\omega_{\rm p} = -100$ Hz, the dotted curve crosses the curve of $\omega = \Omega - \Omega_\perp$. Outside the crossing point, the dotted curve changes into a thick solid curve (i.e., resonance excites oscillations).

one-armed ($m = 1$) corrugation waves at the resonant radii given by equation (1) and the sign of the wave energy of the waves shows that among resonances specified by equation (1) the resonance given by $\omega = \kappa + \omega_{\rm p}$ excites the oscillations. In figure 4, the curve of $\omega = \kappa + \omega_{\rm p}$ is denoted by a thick solid curve when it is in the propagation region ($\omega < \Omega - \Omega\perp$) of the oscillations, while by a dotted curve when it is in the evanescent region. Although two cases of $\omega_{\rm p} = 0$ and $\omega_{\rm p} = -100$ Hz are shown in figure 4, the difference of two curves of $\omega = \kappa + \omega_{\rm p}$ in two cases of $\omega_{\rm p} = 0$ and $\omega_{\rm p} = -100$ Hz is little, when the curves are in the propagation region of the oscillations. In the right-lower corner of figure 4, the curve of $\omega = \kappa + \omega_{\rm p}$ crosses again the curve of $\omega = \Omega - \Omega_\perp$ when $\omega_{\rm p} < 0$, and the curve of $\omega = \kappa + \omega_{\rm p}$ enters into the propagation region of the corrugation waves for large value of r. In order to show this, an enlargement of the right-lower corner of figure 4 is shown in figure 5.

As in the case of inertial-acoustic oscillations, the group velocity of the c-mode oscillations vanishes at the boundary of the propagation and evanescent regions. Hence, we consider that the c-mode oscillations predominantly excited by the resonance are those that satisfy simultaneously $\omega = \Omega - \Omega_\perp$ and $\omega = \kappa + \omega_{\rm p}$. Combination of these two equations gives

$$\kappa = (\Omega - \Omega_\perp) - \omega_{\rm p}. \tag{9}$$

This is the resonant condition for the most predominantly excited c-mode oscillations. The resonant radius determined by this condition is denoted by $r_{\rm corr}$. The frequency of the corrugation waves at this resonant radius is denoted by $\omega_{\rm corr}$, i.e.,

$$\omega_{\rm corr} = (\Omega - \Omega_\perp)_{\rm corr}. \tag{10}$$

Equation (9) is satisfied at two radii when $\omega_{\rm p} < 0$ as is shown in figures 4 and 5. The radius-precession relation specified by equation (9) is shown in figure 3 in the case of $a_* = 0.1$ and 0.3 with $M = 2.0 M_\odot$.

5. Frequency Correlations and Comparison with Observations

Arguments in subsection 4.1 show that the inertial-acoustic oscillations that are dominantly excited on the deformed disks are those whose frequencies are specified by $\omega_{\rm LL}$, $\omega_{\rm L}$, and $\omega_{\rm H}$ [see equations (7) and (8)]. (Oscillations with $\omega_{\rm HH}$ are not considered here, since their frequency is rather high and will be outside of observations.) Among these three oscillations, the oscillation of $\omega_{\rm H}$ will be less important in observational view points. This is because the propagation region of the oscillation is outside the resonant radius $r_{\rm res}$ and extended infinitely. This suggests that the oscillation will not remain for a long time around the resonant radius, since it propagates away outside. On the other hand, the propagation regions of waves with $\omega_{\rm LL}$ and $\omega_{\rm L}$ are inside the resonant radius. The waves are, thus, partially trapped between the resonant radius, $r_{\rm res}$, and the inner edge of the disk, and remain in that region for a long time, different from the wave with $\omega_{\rm H}$.

Next, we should emphasize here that one-armed oscillations with $\omega_{\rm LL}$ are not always observed only with their own frequency $\omega_{\rm LL}$. They may be observed with the two-fold frequency when the disk region where the oscillations are excited is surrounded by a hot corona and when we observe high energy photons that are reprocessed in the corona (see figures 2 – 4 by Kato and Fukue 2006). Based on these two considerations, we think that the frequencies related to the twin HF QPOs observed in black-hole and neutron-star binaries are $2\omega_{\rm LL}$ and $\omega_{\rm L}$.

The corrugation waves that are excited are also one-armed, and thus by the same reason mentioned above they will be observed with the twofold frequency, $2\omega_{\rm corr}$. It is further noted that they are trapped inside the resonant radius, $r_{\rm corr}$.

In summary, we take the picture that the main frequencies to be observed are

$$2\omega_{\rm corr}, \quad 2\omega_{\rm LL}, \quad \omega_{\rm L}, \tag{11}$$

in the order of increase of frequency. As discussed below, $2\omega_{\rm corr}$ will correspond to the low-frequency QPO (LF QPO), and $2\omega_{\rm LL}$ and $\omega_{\rm L}$ correspond to the lower and upper kHz QPOs, respectively.

If the deformation has no precession, the frequency ratio of $2\omega_{\rm LL}$ to $\omega_{\rm L}(=\omega_{\rm H})$ is just 2 to 3, independent of M and a_*. We think that the twin QPOs in black-hole X-ray binaries represent this case (Kato and Fukue 2006).

In the case of neutron-star X-ray binaries, we suppose that the disk deformation has a time-dependent precession as mentioned before (see subsection 2.1). The frequencies $2\omega_{\rm corr}$, $2\omega_{\rm LL}$, and $\omega_{\rm L}$ are thus functions of $\omega_{\rm p}$ as well as M and a_*. Then, rearranging the functional relations, we obtain $2\omega_{\rm corr}$, $\omega_{\rm L}$, and $|\omega_{\rm p}|$ as functions of $2\omega_{\rm LL}$ with parameters a_* and M. As a typical example, these relations are shown in figure 6 for $M = 2.0M_\odot$ and $a_* = 0.3$. It is noted that this figure is drawn for $\omega_{\rm p} < 0$. When $\omega_{\rm p} < 0$, we have two resonant radii for a given $\omega_{\rm p}$ (see figure 3), i.e., an inner resonance and an outer resonance. The curves drawn in figure 6

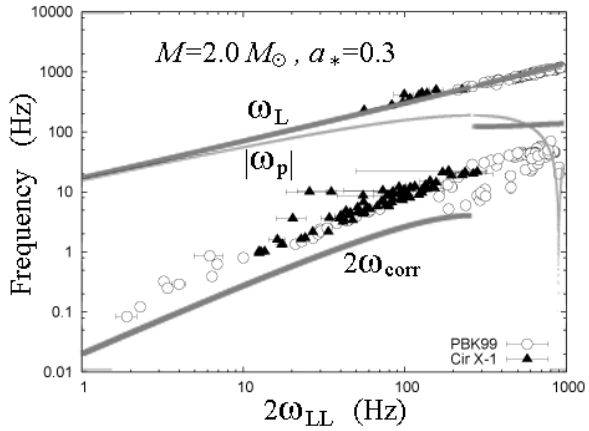

Fig. 6. Diagram showing the $\omega_{\rm L}$ – $2\omega_{\rm LL}$ and $2\omega_{\rm corr}$ – $2\omega_{\rm LL}$ relations in the case of $M = 2.0M_\odot$ and $a_* = 0.3$. The curve of the $|\omega_{\rm p}|$ – $2\omega_{\rm LL}$ relation is also shown by thin curve. Observational data showing the correlation between the upper and lower kHz QPOs and the correlation between the low frequency QPO and the lower kHz QPO (Boutloukos et al. 2006) are superposed. The filled triangles are the data of Cir X-1. The open circles are data of other sources of Psaltis et al. (1999), which have been plotted on Boutloukos et al.'s figure.

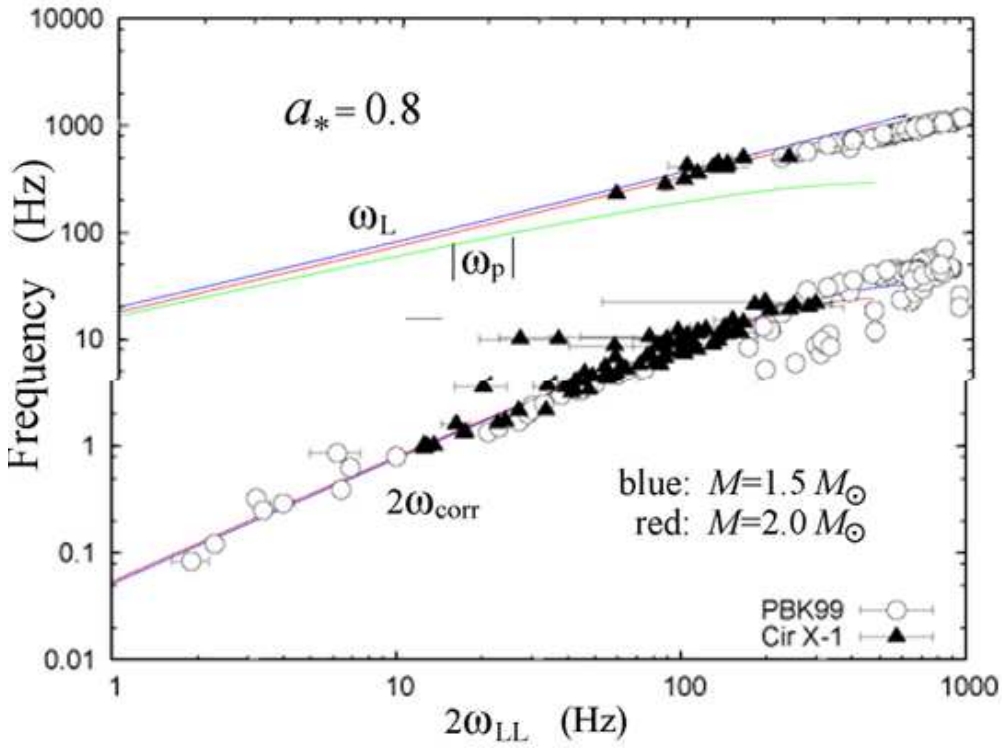

Fig. 7. The same as figure 6, except that two cases of ($M = 1.5M_\odot$, $a_* = 0.8$) and ($M = 2.0M_\odot$, $a_* = 0.8$) are drawn on the same diagram. The blue curves are for ($M = 1.5M_\odot$, $a_* = 0.8$) and the red ones are for ($M = 2.0M_\odot$, $a_* = 0.8$). The green curve represents the precession frequency. The differences between the two curves of $2\omega_{\rm corr}$ are a few, except in the high frequency region.

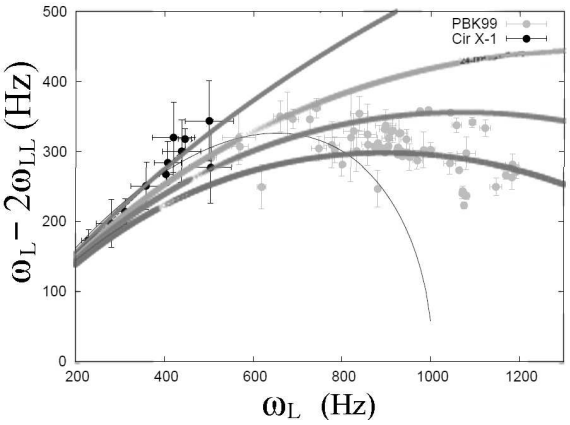

Fig. 8. Diagram showing the $\Delta\omega - \omega_{\rm L}$ relation, where $\Delta\omega$ is the difference between $\omega_{\rm L}$ and $2\omega_{\rm LL}$, i.e., $\Delta\omega = \omega_{\rm L} - 2\omega_{\rm LL} = \kappa_{\rm res}$. Parameters ($M$, a_*) adopted are, from the uppermost to lowermost curves, (2.0, 0.8), (2.0, 0.3), (2.0, 0.0), and (2.4, 0.0). The diagram showing the difference between the upper and lower kHz QPO frequencies versus the upper kHz QPO frequency (Boutloukos et al. 2006) are superposed, assuming that the upper kHz QPO corresponds to $\omega_{\rm L}$. The black circles (they are on the left-hand side of this figure) are the data of Cir X-1 (Boutloukos et al. 2006) and the dark circles are the data of other sources (Psaltis et al. 1999). The thin solid curve is the relativistic precession model by Stella and Vietri (1999) (see Boutloukos et al. 2007).

(and in subsequent figures) are for the frequencies of the outer resonance[4]. On figure 6 the observational data of Cir X-1 (figure 9 of Boutloukos et al. 2006) are superposed, assuming that the frequency of the lower kHz QPO corresponds to $2\omega_{\rm LL}$. The frequency correlations shown in figure 6 seem to qualitatively account for the correlations among observed QPOs of Cir X-1, but there are systematic deviations, especially in the correlation between the $2\omega_{\rm corr}$ – $2\omega_{\rm LL}$ relation and the observed LF QPO – lower kHz QPO relation. We have two adjustable parameters, i.e., M and a_*. The $2\omega_{\rm corr}$ – $2\omega_{\rm LL}$ relation depends strongly on the value of a_*, since $\omega_{\rm corr}$ is related to a small difference between two large quantities of Ω and $\Omega_\perp$, and $\Omega_\perp$ becomes close to Ω with decrease of a_*. On the other hand, the $\omega_{\rm L}$ – $2\omega_{\rm LL}$ relation depends only weakly both on a_* and M. The observed data of Cir X-1 seem to be well described, if $M = 1.5 \sim 2.0 M_\odot$ and $a_* = 0.8$ are adopted, as shown in figure 7. It is noted here that if we adopt $a_* = 0.6$ with $M = 1.5 \sim 2.0 M_\odot$, the $2\omega_{\rm corr}$ – $2\omega_{\rm LL}$ relation runs slightly below the observed LF QPO – lower kHz QPO relation.

In order to see more closely in what parameter cases the $\omega_{\rm L}$ – $2\omega_{\rm LL}$ relation fits the observations, the difference, $\Delta\omega$, between $\omega_{\rm L}$ and $2\omega_{\rm LL}$, i.e., $\Delta\omega \equiv \omega_{\rm L} - 2\omega_{\rm LL} = \kappa_{\rm res}$, is plotted against $\omega_{\rm L}$ in figure 8 for $M = 2.0 M_\odot$ with some values of a_*. For a comparison, the case of $M = 2.4 M_\odot$ and $a_* = 0$ is also shown in figure 8. The observed frequency difference between

[4] The inner resonance has higher frequencies and is inadequate to describe the QPO frequencies observed in Cir X-1. In some sources, kHz QPOs have been observed with higher frequencies, compared with in Cir X-1. Such high frequency QPOs will come from the inner resonance, as discussed in the next section.

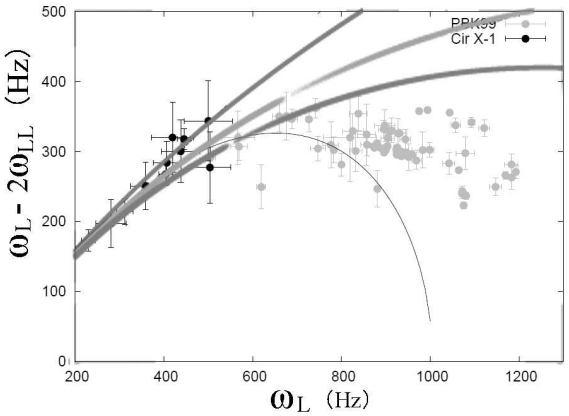

Fig. 9. The same as figure 8 except that $M = 1.7M_\odot$ and $a_* = 0.8$, 0.3, 0.0 from upper to lower.

the upper and lower kHz QPOs versus the upper kHz QPOs in Cir X-1 is given in figure 11 of Boutloukos et al. (2006). The figure of Boutloukos et al. (2006) has been overlapped on figure 8. As another example of comparison, the cases of $M = 1.7M_\odot$ are shown in figure 9 for three cases of $a_* = 0.8$, 0.3, and 0.0. Figures 8 and 9 show that a rather high value of a_*, say $a_* \sim 0.8$, is necessary in the case of Cir X-1 in order to account for the correlation between the twin kHz QPOs. Requirement of such a high value of a_* is compatible with what required in the previous paragraph to describe the LF QPO – lower kHz QPO correlation.

6. Discussion

We have applied a resonantly-excited disk-oscillation model to Cir X-1 in section 5. A comparison of observational data with the model suggests that the spin of the central source of Cir X-1 is rather high, i.e., $a_* \sim 0.8$. Let us roughly estimate the spin frequency $\nu_{\rm s}$ of Cir X-1 by using the estimated value of a_*. If a neutron star is rotating uniformly inside the star with $\nu_{\rm s}$, the specific angular momentum, a, of the star is given by $a = 2\pi\nu_{\rm s} I/cM$, where I is the moment of inertia of the star. Since a_* is related to a by $a_* = (c^2/GM)a$, we have $\nu_{\rm s} = a_*(GM^2/2\pi cI)$, which gives

$$\nu_{\rm s} \sim 1.4 \times 10^3 \Big(\frac{M_0^2}{I_{45}}\Big) a_* \quad \text{(Hz)}, \tag{12}$$

where $M_0 = M/M_\odot$ and $I_{45} = I/10^{45}$. If we take $M_0 = 2$, $M_0/I_{45} = 1$ (e.g., Stella and Vietri 1999), and $a_* = 0.8$, we have $\nu_{\rm s} \sim 2.2 \times 10^3$ Hz. Such a high spin, as well as a high eccentric orbit of Cir X-1, may suggest that the system is young.

Comparison of observations and the model suggests that the disk of Cir X-1 has a retrograde precession and it varies in the range of 100 Hz $\sim$ 200 Hz (see figures 6 and 7). For kHz QPOs to be excited by retrograde precession, the absolute value of the precession must be less than a few hundred Hz (see figure 3). Otherwise, inertial-acoustic oscillations cannot have

resonant interaction with disk deformation, i.e., we have no kHz QPOs. That is, the range of variation of QPO frequencies is related to the magnitude of precession and the range of its variation.

Here, we more closely discuss the relations among precession, resonant radius, and frequency of resonant oscillations. If precession is retrograde and its absolute value is smaller than a critical value, resonance occurs at two different radii for each of inertial-acoustic and corrugation waves (see figure 3). For each case of inertial-acoustic and corrugation waves, we call the resonance at the outer radius an outer resonance, and the resonance at the inner radius an inner resonance (see section 5). In the case of Cir X-1, as shown in section 5, the resonance that can describe observations is the outer one (see also that the gradients of three curves of $|\omega_{\rm p}|$, $\omega_{\rm L}$, and $2\omega_{\rm corr}$ are all positive in figures 6 and 7). In Cir X-1, the frequencies of oscillations resonantly excited at the inner resonance are higher than those observed, as long as conventional mass of neutron stars are adopted. The fact that oscillations at the inner resonance are not observed in Cir X-1 suggests that the inner disk region of Cir X-1 is highly disturbed. One of possible causes of such disturbances will be strong couplings of the inner disk region with the surface of the central source through strong magnetic fields and high spin of the central source.

The cases where the observed twin kHz QPOs are the oscillations excited at the outer resonance will be rare, compared with the cases where they are those excited at the inner resonance, since the twin QPOs in many sources have higher frequencies than those in Cir X-1. That is, in the sources where the high-frequency twin QPOs have really frequencies close to or higher than one kHz, they will be resonant oscillations at the inner resonance and the precession will be small or prograde. It is noted that in the case where the precession is slow or prograde, the outer resonance will be observationally less interesting, since the frequencies excited there are too low or the outer resonance itself is absent (see figure 3).

Let us briefly demonstrate an example in which QPOs occur at the inner resonance. Sco X-1 has twin kHz QPOs in the 800 – 1100 kHz range, a $\sim$45 Hz horizontal-branch oscillation (HBO), and a $\sim$ 6 Hz normal-branch oscillation (NBO). Here, we examine the possibility that the observed twin kHz QPOs correspond to $2\omega_{\rm LL}$ and $\omega_{\rm L}$, and the 45 Hz oscillation to $2\omega_{\rm corr}$, as in the case of Cir X-1. The observed frequencies and their changes of the lower and upper kHz QPOs can be roughly described by assuming that the precession of the disk deformation is prograde and $M \sim 2.4 M_\odot$, when a_* is taken to be zero (see figure 3 of Kato 2007). If a_* is zero, however, there is no corrugation wave ($\omega_{\rm corr} = 0$) and we cannot account for a $\sim$ 45 Hz oscillation by our present model. As mentioned in section 5, the frequency correlation between $2\omega_{\rm LL}$ and $\omega_{\rm L}$ is little affected by changing the value of a_*, while the frequency of $2\omega_{\rm corr}$ is strongly affected by a_*. Hence, by adjusting the value of a_* we can describe a 45 Hz QPO by $2\omega_{\rm corr}$. Our preliminary results show that both frequencies of twin kHz QPOs and of HBO can

be accounted for by our model with $M \sim 2.6 M_\odot$[5] and $a_* \sim 0.15$, the precession being nearly zero or weakly prograde. A $\sim$ 6Hz normal-branch oscillation (NBO) might be a manifestation of the slowly precessing disk deformation required in our model.

It is noted here that we have adopted $2\omega_{\rm corr}$ (not $\omega_{\rm corr}$) and $2\omega_{\rm LL}$ (not $\omega_{\rm LL}$) as frequencies of LF QPO and the lower kHz QPO, respectively. This is, however, not always the case in all sources, unless the disks are surrounded by coronae. Hence, some caution will be necessary when we make comparison of the model with observations. For example, the frequency of LF QPO may be $\omega_{\rm corr}$ in some objects.

Hereafter, we mention the basic assumptions involved in the model, and discuss validity of these assumptions. First, we have assumed that (i) the disk is deformed in an eccentric form ($m_{\rm d} = 1$) in the state when the QPOs are observed. There seems no clear observational evidence for or against this assumption. There are, however, numerical simulations that support a relation between disk deformation and appearance of QPOs. Magnetohydrodynamical simulations of accretion flows by Machida and Matsumoto (2008) show a formation of a torus in the central region of disks and its quasi-periodic deformation into a one-armed form at a certain phase of the flows. They show that this deformation gives rise to a low-frequency quasi-periodic variation of mass accretion rate, and further that in this deformed state, high-frequency QPOs of the order of one hundred Hz appear (the mass is taken to be 10 $M_\odot$). It is not clear, however, whether such disk deformations are related to the disk deformation required in the present disk-oscillation model.

The second requirement involved in the present model is that (ii) the deformation must have a time-dependent precession. This time-dependent precession is necessary to bring about a change of resonant radius and thus to account for the frequency change of QPOs. It is uncertain whether such precession really exists in neutron-star binary sources. By couplings through magnetic and radiation fields, the accretion disks surrounding a neutron star will have strong interaction with the surface of the star. This may be one of possible causes of time-dependent precession of deformed disks (see subsection 2.1). The Papaloizou – Pringle instability in a torus, however, will not be at least the cause of the disk precession in Cir X-1, since the precession required to describe the observations is retrograde. The hectohertz QPOs might be a manifestation of the precession, but if so, it is not clear why they are not always observed in the phases where QPOs appear.

Third, it is assumed that (iii) one-armed ($m = 1$) disk oscillations excited on disks are observed with the two-fold frequency. That is, we assume that the resonant region of the geometrically thin disks where QPOs are excited is surrounded by a hot corona (a torus) and the observed QPO photons are those reprocessed in the corona to higher energy. If such a picture is taken, we can expect the two-fold frequency in the case of one-armed oscillations (see

[5] This value of M is rather high compared with the conventional one adopted as the mass of neutron stars, but will be still in the range allowed theoretically and observationally.

figures 2 – 4 by Kato and Fukue 2006). At the phase when the QPOs are observed in black hole sources (i.e., the very high state), the spectra really show coexistence of a disk component and a corona (a torus). It is uncertain, however, that such corona (torus) exists even in the case of neutron-star X-ray sources, since in the case of neutron stars, a hot corona will be weakened by presence of abundant soft photons from the surface of the star.

Fourth, an important assumption involved in our model is that (iv) dominantly excited oscillations are those with zero group velocity. This is an approximate procedure. In the future, it will be necessary to solve global disk oscillations with relevant boundary conditions in order to clarify whether this approximate procedure is allowed as the first approximation. Another important issue to be reminded here is whether the outward propagation oscillations, characterized by $\omega_{\rm H}$ and $\omega_{\rm HH}$, can be really regarded as less important, compared with the oscillations characterized by $\omega_{\rm LL}$ and $\omega_{\rm L}$.

Unlike the epicyclic resonant model by Abramowicz and Kluźniak (2001) and Kluźniak and Abramowicz (2001), in the present disk-oscillation model, the appearance of the twin QPOs is not a result of mutual interaction of twin oscillations. In the present model, twin oscillations are independently excited by interaction with the disk deformation. In this reason, there is no direct amplitude relation between the twin oscillations in the present model. Török (2008) found a frequency – amplitude relation of the observed twin QPOs. Such correlations cannot be accounted for in this model, unless nonlinear evolutions of the excited oscillations are considered.

Finally, we should notice a close relation between our present model and the relativistic precession model by Stella and Vietri (1999). In the latter model, the upper and lower kHz QPOs are interpreted, respectively, as a frequency of disk rotation, Ω, and periastron precession frequency, $\Omega - \kappa$, at a certain radius, which is a free parameter. In the present disk-oscillation model, the frequency of the upper kHz QPO is $2\Omega - \kappa$ (which is close to Ω), and that of the lower one is $2(\Omega - \kappa)$. In the present mode, the radius specifying these frequencies is the radius of resonance, $r_{\rm res}$, which is determined by coupling between the oscillations and the disk deformation. Further, in the model by Stella and Vietri (1999), the frequency of low-frequency QPO is the nodal precession frequency, $\Omega - \Omega_\perp$, at a radius, which is again a free parameter. In our model the frequency of low-frequency QPO (LF QPO) is the frequency of corrugation waves, which is $\Omega - \Omega_\perp$, but the radius specifying the value of $\Omega - \Omega_\perp$ is the resonant radius given by $r_{\rm corr}$.

The author thanks the referee for invaluable comments on comparison of the model with observations. The author also thanks M. Abramowicz, W. Kluźniak, R. Matsumoto, S. Mineshige, M. Bursa, J. Horak, M. Machida, G. Török, for helpfu discussions during the YITP workshop YITP-W-07-14 on "Quasi-Periodic Oscillations and Time Variabilities of Accretion Flows". This workshop was financially supported by the Yukawa Institute of Theoretical

Physics at Kyoto University.

References

Abramowicz, M. A., & Kluźniak, W. 2001, A&A, 374, L19

Boutloukos, S., van der Klis, M., Altamirano, Klein-Wolt, M., Wijnands, R., Jonker, P.G., & Fender, R.P. 2006, ApJ, 653, 1435

Boutloukos, S., van der Klis, M., Altamirano, D., Klein-Woly, M., Wijnands, 2007, WSPC - Proceedings, astro-ph/0701660v2

Kato, S. 1990, PASJ, 42, 99

Kato, S. 2001, PASJ, 53, 1

Kato, S. 2003, PASJ, 55, 257

Kato, S. 2004, PASJ, 56, 905

Kato, S. 2007, PASJ, 59, 451

Kato, S. 2008, PASJ, 60 in press (arXiv: 0709.2467)

Kato, S., Fukue, J., & Mineshige, S. 1998, Black-Hole Accretion Disks (Kyoto: Kyoto University Press)

Kato, S., Fukue, J., & Mineshige, S. 2008, Black-Hole Accretion Disks – Toward a New paradigm – (Kyoto: Kyoto University Press)

Kato, S. and Fukue, J. 2006, PASJ, 58, 909

Kluźniak, W., & Abramowicz, M. 2001, Acta Phys. Pol. B32, 3605

Li, L.-X., Goodman, J., Narayan, R. 2003, ApJ, 593, 980

Machida, M. and Matsumoto, R. 2008, PASJ submitted

Maloney, P.R., Begelman, M.C., & Pringle, J.E., ApJ, 472, 582

Pringle, J.E. 1992, MNRAS, 258, 811

Pringle, J.E. 1996, MNRAS, 281, 357

Psaltis, D., Belloni, T., and van der Klis M.,1999, ApJ, 520, 262

Stella, L., and Vietri, M. 1999, Phys. Rev. L82, 17

Török, G., 2007, private communication